Spin gapless semiconducting behavior in equiatomic quaternary CoFeMnSi Heusler alloy

Lakhan Bainsla,[1] A. I. Mallick,[1] M. Manivel Raja,[2] A. K. Nigam,[3] B. S. D. Ch. S. Varaprasad,[4] Y. K. Takahashi,[4] Aftab Alam,[1] K. G. Suresh,[1,*] and K. Hono[4]

[1]*Department of Physics, Indian Institute of Technology Bombay, Mumbai 400076, India*

[2]*Defence Metallurgical Research Laboratory, Hyderabad 500058, India*

[3]*DCMPMS, Tata Institute of Fundamental Research, Mumbai 400005, India*

[4]*Magnetic Materials Unit, National Institute for Materials Science, Tsukuba 305-0047, Japan*

(Received 2 October 2014; revised manuscript received 22 February 2015; published 13 March 2015)

In this paper, we report the signature of spin gapless semiconductor (SGS) in CoFeMnSi that belongs to the Heusler family. SGS is a new class of magnetic semiconductors which have a band gap for one spin subband and zero band gap for the other, and thus are useful for tunable spin transport based applications. We show various experimental evidences for SGS behavior in CoFeMnSi by carefully carrying out the transport and spin-polarization measurements. SGS behavior is also confirmed by first-principles band-structure calculations. The most stable configuration obtained by the theoretical calculation is verified by experiment. The alloy is found to crystallize in the cubic Heusler structure (LiMgPdSn type) with some amount of disorder and has a saturation magnetization of 3.7 μ_B/f.u. and Curie temperature of ~620 K. The saturation magnetization is found to follow the Slater-Pauling behavior, one of the prerequisites for SGS. Nearly-temperature-independent carrier concentration and electrical conductivity are observed from 5 to 300 K. An anomalous Hall coefficient of 162 S/cm is obtained at 5 K. Point contact Andreev reflection data have yielded the current spin-polarization value of 0.64, which is found to be robust against the structural disorder. All these properties strongly suggest SGS nature of the alloy, which is quite promising for the spintronic applications such as spin injection as it can bridge the gap between the contrasting behaviors of half-metallic ferromagnets and semiconductors.

DOI: 10.1103/PhysRevB.91.104408 PACS number(s): 85.75.−d, 75.47.Np, 75.76.+j, 76.80.+y

I. INTRODUCTION

In recent studies, a new class of materials known as spin gapless semiconductors (SGSs) has been reported to be promising for spintronic applications [1–3]. SGSs have a band structure in which one spin-polarized subband resembles that of a semiconductor, while the other subband has a zero band gap at the Fermi level (see Fig. 1 for schematics of density of states). Therefore, they combine the band structures of a ferromagnet and a semiconductor. Because of their unique properties, these are being considered as substitutes for diluted magnetic semiconductors (DMSs) and are receiving intense research interest since the theoretical prediction. The major drawback of DMSs is their low Curie temperature [4,5], which can be overcome in many anticipated SGS materials like some Heusler alloys.

For spintronics, Heusler alloys have a special place due to their high Curie temperatures (T_C) and tunable electronic and/or magnetic properties [6]. Many Heusler alloys have been theoretically predicted to exhibit SGS behavior [3,7–9]. However, the inverse Heusler alloy, Mn_2CoAl, is the only material from the Heusler family in which the SGS behavior has been confirmed experimentally [2]. Very recently this alloy has been studied in the thin-film form as well, in order to check the applicability of the material in devices [10,11].

In the case of half-metallic materials, the electronic structure is metallic for one channel and semiconducting for the other channel, and hence the electrical transport is by the electrons with only one type of spin. SGS possess an open band gap for one channel and closed gap for the other channel. When the top of the valence band and the bottom of the conduction band for the majority electrons touch the Fermi level [Fig. 1(d)], the resulting structure gives rise to SGS properties. As it is close to the critical point of zero gap, SGS band structure is very sensitive to external influences, e.g., pressure or magnetic field. The density of states (DOS) schemes for a typical normal metal, semiconductor, half-metallic ferromagnet (HFM), and a SGS are compared in the Fig. 1. Some of the unique properties in the case of SGS are (i) spin-polarized current resulting from electrons as well as spin-polarized holes; (ii) ability to switch between n- or p-type spin-polarized carriers by applying an electric field; (iii) almost no energy required to excite electrons from the valence band to the conduction band.

Conventional full (ternary) Heusler alloys, with the stoichiometric composition A_2CD, where A and C are the transition metals and D is a sp (or main group) element, have the cubic $L2_1$ structure (space group Fm-3m). However, when two ternary Heusler alloys, A_2CD and B_2CD, are combined together to form a quaternary compound $ABCD$ with the stoichiometry 1:1:1:1, they show the LiMgPdSn prototype or the so-called Y-type structure (space group F-43m, #216) with somewhat different symmetry. These quaternary Heusler alloys have been explored only very little for their functional properties [8,12–14]. The compound CoFeMnSi (henceforth referred to as CFMS) can be regarded as the combination of Co_2MnSi and Fe_2MnSi. In the present work, we report strong evidences of SGS behavior for CFMS by carefully examining the alloy using structural, magnetization, spin-polarization, magnetotransport, and Hall effect measurements, supported by *ab initio* calculations.

*Corresponding author: suresh@phy.iitb.ac.in

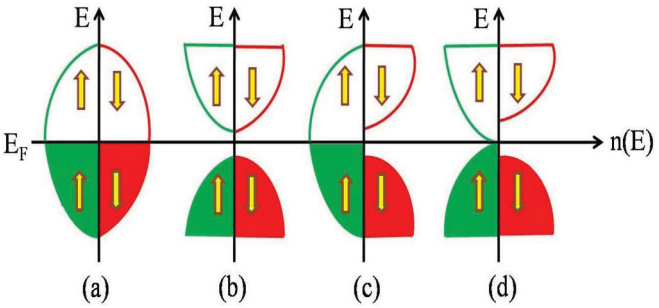

FIG. 1. (Color online) Schematic of density of states for a typical (a) metal, (b) semiconductor, (c) half-metal, and (d) spin gapless semiconductor.

II. EXPERIMENTAL AND COMPUTATIONAL DETAILS

A. Experimental details

The polycrystalline sample of the CFMS alloy was prepared by arc melting of stoichiometric quantities of constituent elements (at least 99.9% purity) in argon atmosphere. The sample was flipped and melted several times to increase the homogeneity and the final weight loss was less than 1%. To further increase the homogeneity, the as-cast sample was annealed under vacuum for 14 days at 1073 K and then quenched in cold water. The crystal structure was investigated by x-ray diffraction pattern (XRD) collected at room temperature using Cu $K\alpha$ radiation. ^{57}Fe Mössbauer spectra were collected at room temperature using a constant acceleration spectrometer with 25 mCi ^{57}Co(Rh) radioactive source. The spectra were analyzed using the PCMOS-II least-squares fitting program. A rectangular piece of $10 \times 5 \times 2\,\text{mm}^3$ has been taken out from the annealed sample for the point contact Andreev reflection (PCAR) measurements. Current spin-polarization measurements were done using the PCAR technique [15]. Sharp Nb tips prepared by electrochemical polishing were used to make point contacts with the sample. Spin polarization of the conduction electrons was obtained by fitting the normalized conductance $G(V)/G_n$ curves to the modified Blonder-Tinkham-Klapwijk (BTK) model [16]. A "multiple parameter least-squares fitting" was carried out to deduce current spin polarization (P) using dimensionless interfacial scattering parameter (Z), superconducting energy gap (Δ), and P as variables. The magnetic and transport measurements were performed in the temperature range of 5–300 K and in fields up to 50 kOe, using the physical property measurement system (PPMS); (Quantum Design).

B. Computational details

First-principles electronic structure calculations were performed with the spin-polarized density functional theory (DFT) within Vienna *ab initio* simulation package (VASP) [17] with a projected augmented-wave basis [18] using generalized gradient approximation (GGA) exchange correlation functional. A Monkhorst-Pack Brillouin-zone integration with $24 \times 24 \times 24\,\mathbf{k}$ mesh was used for the calculation. We have used high precision with large plane-wave cutoffs (340 eV), giving convergence within 10^{-1} meV/cell (10 kBar) for energy (stress tensor). The experimental lattice constant ($a_{\text{expt}} =$ 5.658 Å) obtained in our work has been used for all the calculations. This is done because of various reasons. First of all, it is well known that GGA, in general, yields slightly larger lattice parameters compared to a_{expt}. However, strangely, in this class of intermetallic Heusler compounds, it does the opposite job. The calculated lattice constant comes out to be 1%–2% smaller than a_{expt} (also see Table II of Ref. [13]). Researchers came up with various arguments from time to time and attributed such discrepancies to, e.g., temperature effects (measurement at 300 K, calculation at 0 K), disorder and/or structural defects, electron-electron correlation effects, etc. Electronic structure properties in these classes of systems are extremely sensitive to the details of the calculations (also mentioned in Ref. [13]). In order to avoid such issues, we have used measured lattice parameters (a_{expt}) for our electronic structure calculations so that we can make a one-to-one comparison between theory and experiment.

III. RESULTS AND DISCUSSION

A. Electronic structure calculations

In order to check the phase stability of the structure, we have calculated the site preference energies of various configurations for CFMS. The F-43m crystal structure (with atomic label $ABCD$) is shown in the inset of Fig. 2. The structure can be considered as the four interpenetrating fcc sublattices with Wyckoff positions A(0,0,0), B(1/4,1/4,1/4), C(1/2,1/2,1/2), and D(3/4,3/4,3/4). Considering the symmetry of the structure, we fixed the position of Si atom at D sites and all combinations of the other three elements (in total six configurations) were checked. Out of six possible configurations, only four configurations are distinct and the rest two are energetically degenerate. The site preference energy of the four distinct configurations is shown in Fig. 2. E_0 is just a reference energy, which corresponds to the most stable configuration (Type 4). The two degenerate configurations are Type 5: Co, A; Fe, B; Mn, C (equivalent to Type 3)

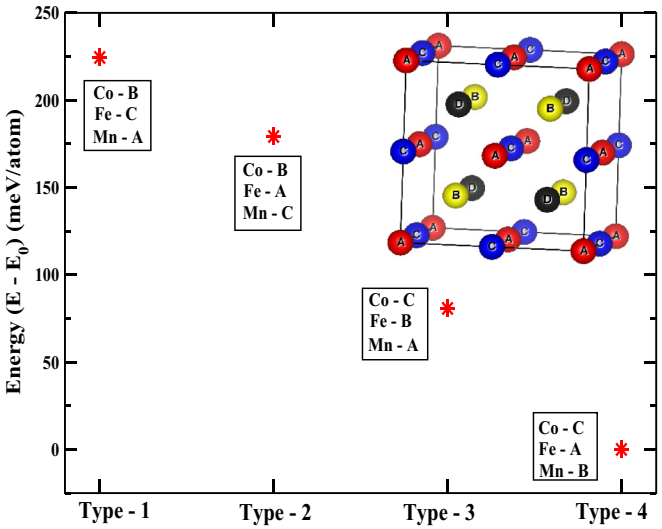

FIG. 2. (Color online) Site preference energies for different configurations of CoFeMnSi. Inset: crystal structure of prototype LiMgPdSn.

and Type 6: Co, A; Fe, C; Mn, B (equivalent to Type 4). These calculations give an accurate idea about the most favorable occupancy scheme of the constituent atoms in CFMS. The calculated magnetic moments for the energetically most favorable configuration [i.e., Type 4: Co, C; Fe, A; Mn, B; and Si, D or Type 6 (equivalent to Type 4): Co, A; Fe, C; Mn, B; and Si, D] are $\mu_{\mathrm{Co}} = 0.82\,\mu_B$/atom, $\mu_{\mathrm{Fe}} = 0.53\,\mu_B$/atom, $\mu_{\mathrm{Mn}} = 2.72\,\mu_B$/atom. The total magnetic moment per cell is found to be $\mu_{\mathrm{Tot}} = 4.01\,\mu_B$, which follows the Slater-Pauling behavior [19]. Experimentally, our structural analysis also revealed that the alloy exists in the Type 6 configuration.

Figure 3 shows the calculated spin-polarized band structure and the density of states of the energetically most favorable configuration (Type 4 or Type 6). One can notice that the DOS exhibits a band gap ~0.62 eV (semiconducting behavior) in one spin subband, while the Fermi level falls within a negligible energy gap in the other spin subband. The minority-spin band structure indicates a band gap between the t_{2g} and e_g states, which resembles the band structure of other nonmagnetic semiconductors. Notably, the band structure for the majority-spin band shows an indirect nature of the gap, where the valence band at Γ almost touches the conduction band at X, which corresponds to a deep valley in the DOS at E_F. Such a nearly closed band gap character in one spin channel suggests CFMS to be a close spin gapless semiconductor. Xu *et al.* [7] also predicted CFMS to be a spin gapless semiconductor from another *ab initio* calculation.

SGS state lies in between a half-metallic and a semiconducting state and hence is very difficult to probe. Therefore, it requires very careful measurements and *ab initio* calculations to accurately ascertain this behavior in a material. For instance, Alijani *et al.* [13] proposed CFMS to be a half-metal on the basis of simple magnetic measurement and hard x-ray photoelectron spectroscopy. First of all, such measurements (merely satisfying the Slater-Pauling rule) or x-ray photoelectron spectroscopy measurements may not give a concrete idea about the metallicity or semiconducting behavior of a material. A more reliable information about such a behavior of a material (especially sensitive compounds like CFMS, which is very close to being SGS) can only be obtained from transport and spin-polarization measurements, as done in the present work.

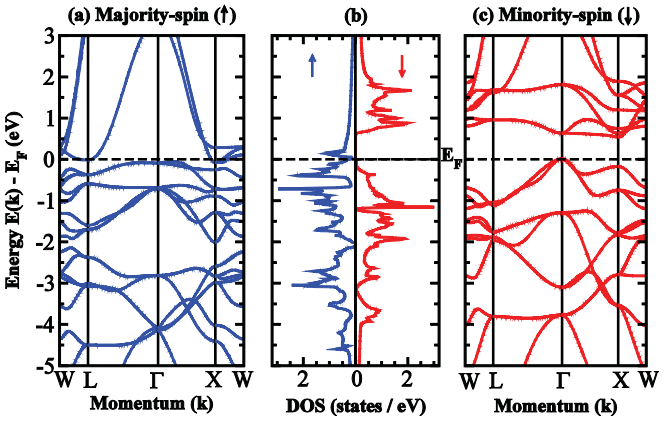

FIG. 3. (Color online) Band structure and density of states of CoFeMnSi: (a) majority-spin bands, (b) density of states, (c) minority-spin bands.

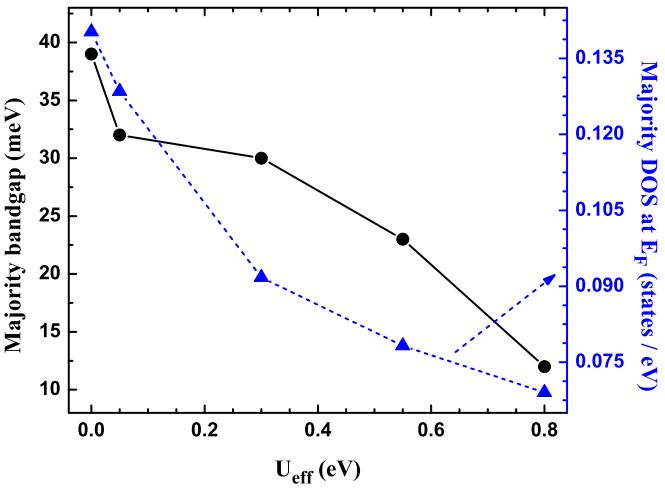

FIG. 4. (Color online) Band gap and minimum value of DOS near the Fermi level in the majority-spin channel vs U_{eff} ($= U - J$) with different U and fixed J (=0.2 eV) values. U_{eff} is applied only on the d electrons of Mn because of its dominant effect.

To check the effect of localized d electrons of transition-metal elements on the total density of states of the compound near the Fermi level, we have used the GGA + U approach [20] with Hubbard U introduced in a screened Hartree-Fock manner. It is found that the effect of Hubbard U on Co and Fe d electrons is negligibly small and considerable effect comes only from the d electrons of Mn ions. So, we have done the self-consistent calculations using GGA + U only on Mn d electrons whereas all other components were treated within GGA only. The variations of band gap in the majority-spin state and the minimum value of total DOS near Fermi level with different U_{eff} ($= U - J$) are shown in Fig. 4.

B. Structural analysis

The superlattice reflections were clearly observed in the XRD pattern, which reveal that the alloy exists in ordered cubic Heusler structure (LiMgPdSn type) with F-43m space group (#216). The lattice parameter of the alloy was found to be $a = 5.658$ Å from the Rietveld refinement, which is in close agreement with the earlier report [13]. Further information about the crystal structure was derived with the help of ^{57}Fe Mössbauer spectroscopic measurements at room temperature as shown in the Fig. 5. The experimental Mössbauer spectrum has been fitted with three sextets (S_1, S_2, S_3) having hyperfine field (H_{hf}) values of 290, 132, and 98 kOe and also a doublet with the relative intensities of 38%, 35%, 17%, and 10%, respectively. The quadrupole shift value is almost zero, which is in accordance with the cubic symmetry of local Fe environment. The best fit of the spectrum was obtained by considering the Type 6 configuration (which is equivalent to Type 4) in LiMgPdSn structure. For a well-ordered LiMgPdSn structure, Fe atoms must occupy the C sites with cubic symmetry (O_h) resulting in a single sextet because there is only one crystallographic site for Fe. The presence of three sextets indicates some amount of structural disorder in the alloy. A large decrease in H_{hf} is expected when Fe occupies B and D sites because the number of magnetic near neighbors is different in these two cases; H_{hf} is expected to not change

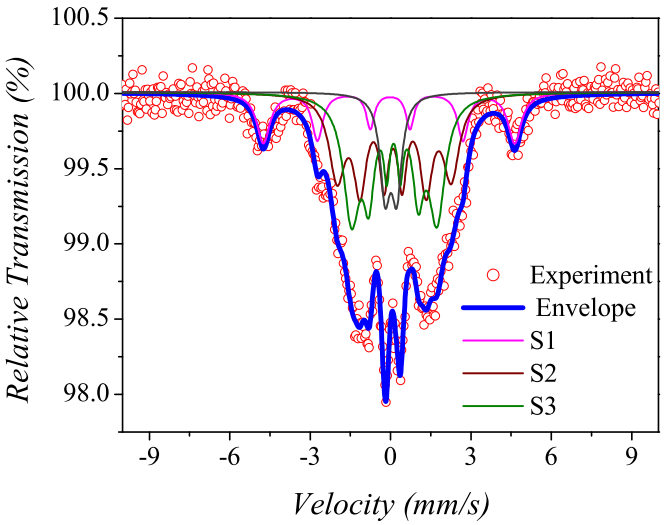

FIG. 5. (Color online) ^{57}Fe Mössbauer spectrum of CFMS collected at room temperature.

much when Fe occupies the A site as the number of magnetic near neighbors is similar for A and C sites. The experimentally observed value of H_{hf} clearly indicates that Fe also occupies B, D sites, resulting in DO_3 type disorder. The subspectra S_1, S_2, and S_3 are ascribed to the ordered LiMgPdSn phase, DO_3 (C site), and DO_3 (B site) phases, respectively. The intensity of S_1 (38%) is found to be higher as compared to S_2 (35%) and S_3 (17%), which implies that the structure is reasonably ordered at room temperature. The structural stability of the alloy was checked using differential thermal analysis (DTA) in the temperature range of 400–1450 K. The DTA plot shows no structural transitions, indicating the structural stability in the entire temperature range investigated. A minimum in the DTA exothermic curves was observed near the Curie temperature ($T_C \approx 620$ K), which is in agreement with earlier observation of 623 K [13].

C. Electrical conductivity and Hall measurements

The temperature dependencies of the electrical conductivity [$\sigma_{xx}(T)$] and the carrier concentration [$n(T)$] are shown in Fig. 6(a). $\sigma_{xx}(T)$ is measured under 0 and 50 kOe fields in the temperature range of 5–300 K. Electrical conductivity increases with increase in temperature, indicating a nonmetallic conduction. $\sigma_{xx}(T) = 2980$ and 3000 S/cm are obtained at temperature of 300 K under the field of 0 and 50 kOe, respectively. The electrical conductivity value obtained at 300 K for CFMS is slightly higher than that reported for Mn_2CoAl (i.e., 2440 S/cm) [2]. $\sigma_{xx}(T)$ varies linearly in the high-temperature region, while a nonlinear behavior is observed in the low-temperature region. The disorder-enhanced coherent scattering of conduction electrons may be the cause for the nonlinear behavior at low temperatures [21]. The conductivity behavior is unusual and different from that of the normal metals or semiconductors. Carrier concentration of the CFMS alloy is calculated from the Hall coefficient (R_H) measurements. The temperature-independent carrier concentration (n) is observed in the temperature range from 5 to 300 K, which is typical of spin gapless semiconductors [2,22]; carrier concentration of 4×10^{19} cm^{-3} is observed at 300 K, which is comparable to that observed for HgCdTe (10^{15}–10^{17} cm^{-3}), Mn_2CoAl (10^{17} cm^{-3}), and Fe_2VAl (10^{21} cm^{-3}) [23]. The physical reasons for the nearly temperature-independent carrier concentration in gapless semiconductors as compared to the exponential dependence in the case of conventional semiconductors are well established [22,24]. The carrier concentration in the case of gapless semiconductors varies as [22]

$$n_i = p_i = 2m_e m_h^{1/2} \left[\frac{k_B T}{2\pi\hbar^2}\right]^{3/2}, \qquad (1)$$

where m_e and m_h are the effective masses of the electrons and holes. A good fit to this expression, as shown in Fig. 7, reveals the spin gapless semiconducting behavior in CFMS. Therefore, the behavior of $\sigma_{xx}(T)$ and $n(T)$ strongly supports the SGS behavior in this material. The observations of low carrier concentration and high resistivity show the exceptional stability of electronic structure and its insensitivity to the structural disorder in this alloy.

The anomalous Hall conductivity $\sigma_{xy} = \rho_{xy}/\rho_{xx}^2$ at 5 K was obtained from the magnetic field–dependent transport measurements in order to study the low-field behavior in more

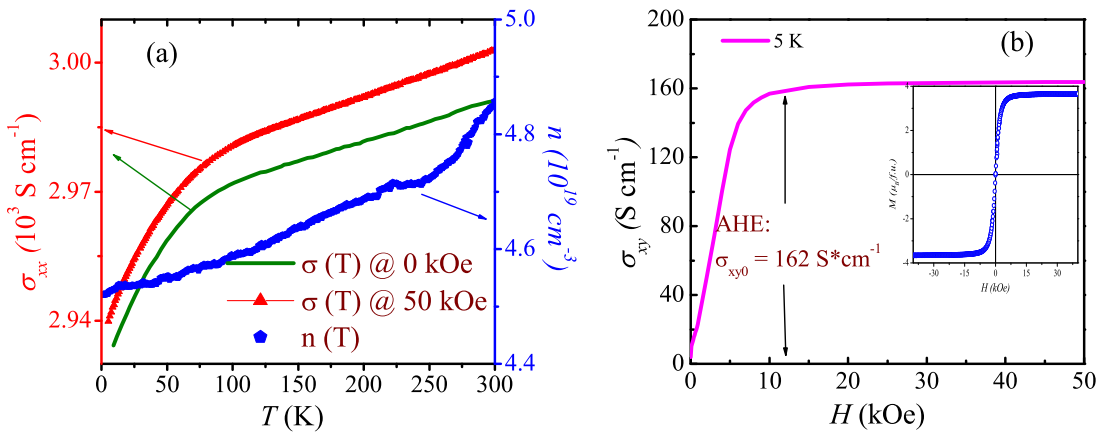

FIG. 6. (Color online) (a) Temperature dependence of the electrical conductivity; $\sigma_{xx}(T)$ (left-hand scale); variation of carrier concentration, $n(T)$ with temperature (right-hand scale). (b) Representation of the field dependence of anomalous Hall effect (AHE) at 5 K. The Hall conductivity, $\sigma_{xy}(T)$ is shown as the function of applied field. Inset in (b) shows the magnetization isotherm obtained at 5 K.

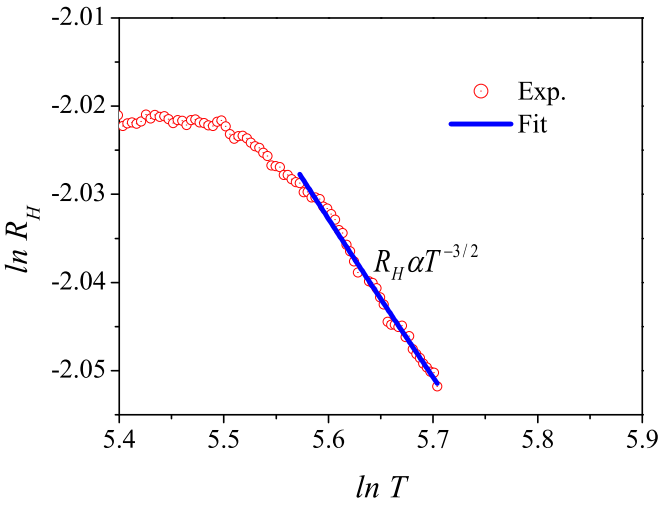

FIG. 7. (Color online) Temperature dependence of Hall coefficient (R_H) for CFMS alloy.

detail. Hall conductivity follows the same behavior as observed for the magnetization isotherm (inset) as shown in Fig. 6(b). The anomalous Hall conductivity (σ_{xy0}) value is defined as the difference in σ_{xy} values at zero and the saturation fields. It is found that σ_{xy0} attains a value of 162 S/cm, which is higher than that observed in Mn_2CoAl (22 S/cm) [2], but less than that of the half-metallic Co_2FeSi (≈200 S/cm at 300 K) [25], and Co_2MnAl (≈2000 S/cm) [26]. As can be seen from the inset of Fig. 6(b), the saturation magnetization (M_S) value of 3.7 μ_B/f.u. is obtained at 3 K, which is less than the calculated value of 4.01 μ_B/f.u. The structural disorder observed from the Mössbauer data may be the reason behind the disagreement between the observed and calculated values of M_S.

D. Spin polarization

The current spin-polarization (P) measurements at the ferromagnetic (FM)-superconductor (SC) point contact were done by using the PCAR technique [15]. All the conductance curves (Fig. 8) were recorded at the temperature of 4.2 K by using Nb as the superconducting tip. The normalized conductance curves were fitted to the BTK model [16] by keeping P, Δ, and Z as variables. Due to the absence of proximity effect in the PCAR data, we assumed $\Delta = \Delta_1 = \Delta_2$. The values of fitted parameters with best fitting (smallest χ^2 value) are shown in the figures. The shape of the conductance curves depends on the value of Z, with the curves becoming flat near the Δ for low Z values. The values of Δ obtained from the best fit are lower than the bulk superconducting band gap of Nb = 1.5 meV, which is due to the multiple contacts at the interface [27]. The intrinsic value of current spin polarization is obtained by recording the conductance curve for $Z = 0$. However, in the present case, the lowest possible Z value was 0.10 and therefore, the P vs Z plot was extrapolated to $Z = 0$. The current spin-polarization value of 0.64 is deduced from the P vs Z plot, which is comparable to the value obtained in some high-spin-polarization materials by using the PCAR technique such as $Co_2Fe(Ga_{0.5}Ge_{0.5})$ with $P = 0.69 \pm 0.02$ [28], $Co_2Fe(Al_{0.5}Si_{0.5})$ with $P = 0.60 \pm 0.01$ [29], and CoFeMnGe with $P = 0.70 \pm 0.01$ [12].

In the measurement of P by PCAR, one measures the conductance curves across the ferromagnetic (FM)-superconductor (SC) contact and the spin polarization for a ballistic contact can be expressed as the imbalance in the majority- and minority-spin currents [30], $P = [N_\uparrow(E_F)v_{F\uparrow} - N_\downarrow(E_F)v_{F\downarrow}]/[N_\uparrow(E_F)\,v_{F\uparrow} + N_\downarrow(E_F)v_{F\downarrow}]$. However, the spin polarization of density of states can also be expressed as $P_a = [N_\uparrow(E_F) - N_\downarrow(E_F)]/[N_\uparrow(E_F) + N_\downarrow(E_F)]$, where $N_{\uparrow(\downarrow)}(E_F)$ and $v_{F\uparrow(\downarrow)}$ are the DOS at the Fermi level and the Fermi velocity for spin-up (-down) electrons, respectively. The values of P and P_a are the same when the Fermi velocities of both the spin currents are equal [30]. Hence, DOS at E_F is not the only quantity which controls the spin polarization. Using the numerical values of DOS and Fermi velocities (calculated from the slope of the band near E_F), an approximate theoretical estimate of P comes out to be $P = 0.69$, which compares fairly well with experiment ($P = 0.64$). Spin polarization (P) measured by PCAR is the transport spin polarization, which is the most realistic and relevant parameter from an application point of view in spintronic devices.

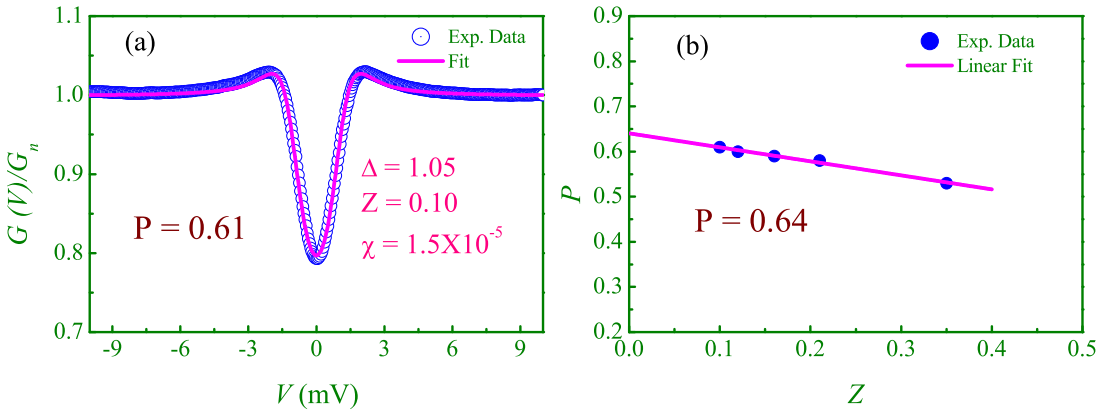

FIG. 8. (Color online) Normalized conductance curves recorded at 4.2 K. In (a) open circles denote the measured experimental data and solid lines are the fit to the data by using modified BTK model. (b) Representation of the linear fit to P vs Z data with extrapolation down to $Z = 0$.

IV. CONCLUSIONS

In conclusion, we address the signature of SGS behavior in the quaternary Heusler alloy CoFeMnSi by providing various experimental and theoretical evidences. *Ab initio* calculations predict the SGS type of electronic structure with open gap for one spin subband and closed (negligibly small) for the other spin band. The phase stability of the alloy was checked by the site preference energies; Type 4 configuration (equivalent to Type 6) is found to be the most stable state. Total magnetization from *ab initio* calculation is found to follow the Slater-Pauling behavior, which is one of the prerequisites for SGS. In order to check the proposed SGS behavior, the alloy was probed by structural, magnetic, magnetotransport, spin-polarization, and Hall effect measurements. The structural analysis reveals that the alloy exists in cubic Heusler structure (prototype LiMgPdSn) with Type 4 configuration, which is also confirmed by the *ab initio* calculation. M_S value at 3 K is found to be 3.7 μ_B/f.u. and the Curie temperature is estimated to be $\approx$620 K. Low values ($\sim 10^{19}$ cm^{-3}) and nearly-temperature-independent carrier concentration along with the electrical conductivity of the order of 3×10^{-3} S/cm illustrates the SGS behavior in this alloy. The current spin-polarization value of 0.64 is deduced from the PCAR conductance curves at 4.2 K. The above-mentioned magnetic and transport properties of this SGS material seem to be very promising for spintronic applications such as spin injection into semiconductors. One of our immediate endeavors is to theoretically investigate the effect of antisite defects, which show some evidence in our Mössbauer spectra.

ACKNOWLEDGMENTS

One of the authors, L.B., would like to thank UGC, Government of India, for granting a senior research fellowship (SRF). K.G.S. thanks ISRO, Government of India, for the financial assistance in carrying out this work. A.I.M. acknowledges the support from TAP fellowship under SEED Grant (Project Code No. 13IRCCSG020). The authors thank D. Buddhikot for his help in the resistivity and Hall measurements.

[1] X. L. Wang, Phys. Rev. Lett. **100**, 156404 (2008).
[2] S. Ouardi, G. H. Fecher, C. Felser, and J. Kübler, Phys. Rev. Lett. **110**, 100401 (2013).
[3] S. Skaftouros, K. Özdogan, E. Sasioglu, and I. Galanakis, Appl. Phys. Lett. **102**, 022402 (2013).
[4] H. Ohno, Science **281**, 951 (1998).
[5] M. Wang, R. P. Campion, A. W. Rushforth, K. W. Edmonds, C. T. Foxon, and B. L. Gallagher, Appl. Phys. Lett. **93**, 132103 (2008).
[6] K. Inomata, N. Ikeda, N. Tezuka, R. Goto, S. Sugimoto, M. Wojcik, and E. Jedryka, Sci. Technol. Adv. Mater. **9**, 014101 (2008).
[7] G. Z. Xu, E. K. Liu, Y. Du, G. J. Li, G. D. Liu, W. H. Wang, and G. H. Wu, Europhys. Lett. **102**, 17007 (2013).
[8] K. Özdogan, E. Sasioglu, and I. Galanakis, J. Appl. Phys. **113**, 193903 (2013).
[9] G. Y. Gao and K. L. Yao, Appl. Phys. Lett. **103**, 232409 (2013).
[10] G. Z. Xu, Y. Du, X. M. Zhang, H. G. Zhang, E. K. Liu, W. H. Wang, and G. H. Wu, Appl. Phys. Lett. **104**, 242408 (2014).
[11] M. E. Jamer, B. A. Assaf, T. Devakul, and D. Heiman, Appl. Phys. Lett. **103**, 142403 (2013).
[12] L. Bainsla, K. G. Suresh, A. K. Nigam, M. Manivel Raja, B. S. D. Ch. S. Varaprasad, Y. K. Takahashi, and K. Hono, J. Appl. Phys. **116**, 203902 (2014).
[13] V. Alijani, S. Ouardi, G. H. Fecher, J. Winterlik, S. S. Naghavi, X. Kozina, G. Stryganyuk, C. Felser, E. Ikenaga, Y. Yamashita, S. Ueda, and K. Kobayashi, Phys. Rev. B **84**, 224416 (2011).
[14] P. Klaer, B. Balke, V. Alijani, J. Winterlik, G. H. Fecher, C. Felser, and H. J. Elmers, Phys. Rev. B **84**, 144413 (2011).
[15] R. J. Soulen, J. M. Byers, M. S. Osofsky, B. Nadgorny, T. Ambrose, S. F. Cheng, P. R. Broussard, C. T. Tanaka, J. Nowak, J. S. Moodera, A. Barry, and J. M. D. Coey, Science **282**, 85 (1998).
[16] G. J. Strijkers, Y. Ji, F. Y. Yang, C. L. Chien, and J. M. Byers, Phys. Rev. B **63**, 104510 (2001).
[17] G. Kresse and J. Furthmuller, Phys. Rev. B **54**, 11169 (1996); Comput. Mater. Sci. **6**, 15 (1996).
[18] G. Kresse and D. Joubert, Phys. Rev. B **59**, 1758 (1999).
[19] I. Galanakis, P. H. Dederichs, and N. Papanikolaou, Phys. Rev. B **66**, 174429 (2002).
[20] S. L. Dudarev, G. A. Botton, S. Y. Savrasov, C. J. Humphreys, and A. P. Sutton, Phys. Rev. B **57**, 1505 (1998).
[21] P. A. Lee and T. V. Ramakrishnan, Rev. Mod. Phys. **57**, 287 (1985).
[22] I. M. Tsidilkovski, *Electron Spectrum of Gapless Semiconductors*, Springer Series in Solid-State Sciences Vol. 116 (Springer, Berlin, New York, 1996).
[23] V. I. Okulov, V. E. Arkhipov, T. E. Govorkova, A. V. Korolev, and K. A. Okulova, Low Temp. Phys. **33**, 692 (2007).
[24] F. S. Pool, J. Kossut, U. Debska, and R. Reifenberger, Phys. Rev. B **35**, 3900 (1987).
[25] D. Bombor, C. G. F. Blum, O. Volkonskiy, S. Rodan, S. Wurmehl, C. Hess, and B. Büchner, Phys. Rev. Lett. **110**, 066601 (2013).
[26] E. V. Vidal, G. Stryganyuk, H. Schneider, C. Felser, and G. Jakob, Appl. Phys. Lett. **99**, 132509 (2011).
[27] S. K. Clowes, Y. Miyoshi, O. Johannson, B. J. Hickey, C. H. Marrows, M. Blamire, M. R. Branford, Y. V. Bugoslavsky, and L. F. Cohen, J. Magn. Magn. Mater. **272**, 1471 (2004).
[28] B. S. D. Ch. S. Varaprasad, A. Srinivasan, Y. K. Takahashi, M. Hayashi, A. Rajanikanth, and K. Hono, Acta Mater. **60**, 6257 (2012).
[29] T. M. Nakatani, A. Rajanikanth, Z. Gercsi, Y. K. Takahashi, K. Inomata, and K. Hono, J. Appl. Phys. **102**, 033916 (2007).
[30] I. I. Mazin, Phys. Rev. Lett. **83**, 1427 (1999).